THE JOURNAL OF PHYSICAL CHEMISTRY B

Article

pubs.acs.org/JPCB

# Dynamics in a Water Interfacial Boundary Layer Investigated with IR Polarization-Selective Pump−Probe Experiments

Rongfeng Yuan, Chang Yan, Jun Nishida, and Michael D. Fayer*

Department of Chemistry, Stanford University, Stanford, California 94305, United States

**ABSTRACT:** The dynamics of water molecules near the surfactant interface in large Aerosol-OT reverse micelles (RMs) ($w_0$ = 16−25) was investigated with IR polarization-selective pump−probe experiments using the $SeCN^-$ anion as a vibrational probe. Linear absorption spectra of RMs ($w_0$ = 25−2) can be decomposed into the weighted sum of the $SeCN^-$ spectra in bulk water and the spectrum of the $SeCN^-$ anion interacting with the interfacial sulfonate head groups ($w_0$ = 1). The spectra of the large RMs, $w_0 \geq 16$, are overwhelmingly dominated by the bulk water component. Anisotropy decays (orientational relaxation) of the anion for $w_0 \geq 16$ displayed bulk water relaxation (1.4 and 4.5 ps) plus an additional slow decay with a time constant of ∼13 ps. The amplitude of the slow decay was too large to be associated with $SeCN^-$ in contact with the interface on the basis of the linear spectrum decomposition. The results indicate that the observed slow components arise from $SeCN^-$ in a water boundary layer, in which water molecules are perturbed by the interface but are not directly associated with it. This layer is the transition between water in direct contact with the interface and bulk water in the large RM cores. In the boundary layer, the water dynamics is slow compared to that in bulk water.

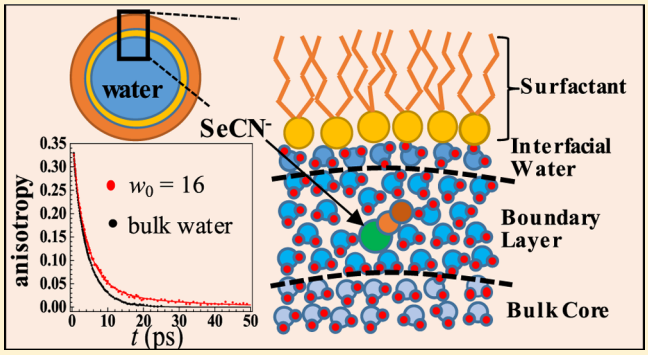


## I. INTRODUCTION

Water is a fundamental component of many natural and man-made systems. In many processes, water does not occur as bulk liquid but rather interacts with interfaces. In biology, water exists in crowded environments, such as cells, where it hydrates membranes and large biomolecules. In geology, ion adsorption and mineral dissolution are controlled by interfacial water molecules. In chemistry, water plays an important role as a polar solvent that is often in contact with interfaces, for example, in ion-exchange resin systems.

The hydrogen-bonding properties of water are distinct from those of bulk water when it interacts with an interface. Interfacial interactions influence the ability of water to undergo hydrogen bond rearrangement, which is a concerted process that involves a water molecule and at least its two water solvation shells.[1,2] For a water molecule to undergo hydrogen bond rearrangement, other water molecules must break and form new hydrogen bonds.[1,2] Such hydrogen bond rearrangements are necessary for both orientational and translational motions. An interface eliminates many of the pathways for hydrogen bond rearrangement that are available in bulk water. It is well established that water molecules in contact with a hydrophilic interface have dynamics that is very different from, that is, substantially slower, that of bulk water.[1,2] It is also well-known that far enough from an interface water has bulk properties.[1]

If water has distinct dynamics when in contact with an interface and consists of bulk water when far from an interface, there must be a transition region between interfacial and bulk water. In this article, we address the important questions of the dynamics in the interfacial boundary layer.

To investigate the interfacial boundary layer, experiments were conducted on reverse micelles (RMs). An RM consists of a nanoscopic water pool surrounded by a layer of surfactants in an organic solvent. The hydrophilic head groups of the surfactants face toward the water pool, whereas the hydrophobic tails merge into the organic phase. The interface between water and the surfactants has attracted a good deal of attention. Tailoring the properties of surfactants leads to diverse surface properties and a broad range of applications, for example, hosting catalytic reactions[3−5] and serving as biological membrane model systems.[6,7]

One of the most commonly used and well-characterized RMs is formed using the surfactant sodium bis(2-ethylhexyl) sulfosuccinate, also known as Aerosol-OT or AOT. The AOT system makes essentially monodispersed and spherical RMs. The size of the water nanopools can be controlled by changing the $w_0$ parameter,[8−10] which is defined as $[H_2O]/[AOT]$, where $[H_2O]$ and [AOT] are the molar concentrations. To examine the dynamics of the water molecules inside the RMs, a variety of techniques have been applied, including nuclear magnetic resonance spectroscopy,[11,12] fluorescence,[13−15] neutron scattering,[16,17] dielectric relaxation,[18] molecular dynamics (MD) simulations,[19,20] and ultrafast IR spectroscopy.[21−24]

**Received:** February 1, 2017
**Revised:** March 23, 2017
**Published:** April 5, 2017





DOI: 10.1021/acs.jpcb.7b01028
J. Phys. Chem. B 2017, 121, 4530−4537

Ultrafast IR spectroscopy is particularly useful because its time resolution allows the dynamics to be directly observed on a picosecond time scale. Using the optical density (OD) stretch of dilute HOD in $H_2O$ as a probe, Moilanen et al. applied the Fourier transform infrared (FT-IR) and IR pump−probe experiments on RMs ranging in size from small ($w_0$ = 2) to large ($w_0$ = 60).[1,23,25] From the IR pump−probe measurements on large RMs ($w_0 \geq 16$), two populations of HODs were observed, which had distinct vibrational lifetimes and reorientation dynamics. The observations can be described by a core/shell model. The "core" region is separated from the interface and has bulk water properties. The OD stretch in this ensemble of water molecules has a vibrational lifetime of 1.8 ps and an orientational relaxation time of 2.6 ps, which are identical to those of bulk water.[26] The other ensemble, the shell, was shown to be hydrogen bonded to the sulfonate AOT head groups. These interfacial water molecules have an OD stretch lifetime of 4.3 ps and an orientational relaxation time constant of 18 ps. The interfacial shell was found to have a width of 0.26 nm, which is close to the diameter of a single water molecule. Therefore, the interfacial shell probably corresponds to water molecules directly.

In large RMs, between the interfacial water and bulk water core there must be a boundary layer that is the transition between them. In contrast to the interfacial layer, in which water molecules are hydrogen bonded to sulfonate AOT head groups, the boundary layer water molecules are hydrogen bonded to other water molecules. However, some of the boundary layer water is hydrogen bonded to the interfacial water molecules. As the dynamics of the interfacial water is very different from that of bulk water, water bound to the interfacial water will have dynamics that differs from that of bulk water. As the distance from the interface increases, the influence of the interface will decrease, and at some distance the water will have bulk properties.

In this paper, we employ ultrafast IR polarization-selective pump−probe (PSPP) experiments performed on a small anionic vibrational probe, the CN stretch of $SeCN^-$, to investigate water dynamics in large RMs. It has been shown with ultrafast IR experiments that $SeCN^-$ reports on water hydrogen bond dynamics.[27] $SeCN^-$ has a substantially longer vibrational lifetime (37 ps) than either the OD (1.8 ps[26]) or OH (0.7 ps[28]) hydroxyl stretches of HOD in $H_2O$ or $D_2O$, respectively, which makes it a useful probe. Experiments using HOD have provided detailed information on orientational relaxation and spectral diffusion in bulk water. Using $SeCN^-$ as the vibrational probe makes it possible to obtain data at much longer times than that possible using HOD.

PSPP experiments on $SeCN^-$ in large RMs, $w_0$ = 16, 20, and 25, yielded orientational relaxation with three components, two of which are identical to those found in bulk water ($D_2O$, 1.4 and 4.5 ps) and an additional decay of ∼13 ps. This slow decay was found in all three of the large RMs. FT-IR experiments showed that the $SeCN^-$ anions that give rise to this slow component are not directly associated with the interface and are therefore assigned to $SeCN^-$ in the boundary layer.

Abel et al. conducted MD simulations on AOT RMs and determined the radial density function of water molecules that suggested the boundary layer is ∼1.0 nm, although the largest RM in the study was $w_0$ = 16.[29] Atomic force microscopy techniques were used on amorphous silica to study thin films of water between two interfaces on a nanometer distance scale and a much larger viscosity was found "than that of bulk water for nanometer-scale interfacial separations".[30] A study of the silica surface as a function of relative humidity using attenuated total reflection IR spectroscopy showed icelike water up to a three-layers thickness for 0−30% relative humidity and an additional layer of liquid water structure, in the humidity range of 30−60%.[31] Water on the hydrophobic surface of mica was studied using high-resolution X-ray specular reflectivity of the mica(001)−water interface. Density oscillations were found to extend to ∼1 nm from the surface and were interpreted as being "due to the "hard-wall" effect of the molecularly smooth mica surface".[32] Singh et al. used tricyanomethanide anions as the vibrational probe for two-dimensional (2D) IR spectroscopy experiments in RMs with $w_0$ values ranging from 4 to 30. Using a heterogeneous dynamics distribution model, they argued that the characteristic decay length, over which the interfacial water dynamics exponentially changes into the bulk value, ranges from 6 Å for $w_0$ = 4 to 0.4 Å for $w_0$ = 30.[33] The exponential decay for $w_0$ = 30 gives the width of the layer influenced by the interface as ∼2 Å, which is less than the size of one water molecule and much smaller than the tricyanomethanide probe molecule. The experiments on the $SeCN^-$ vibrational probe reported here for large RMs examine samples that have an interface and a bulk water core removed from the interface. There is a transition region, a boundary layer between the interface and core. We observe both bulk water dynamics and dynamics that differs from that of the bulk, in addition to very slow dynamics that are associated with the vibrational probe directly interacting with the interface. The results provide information on the dynamics in the boundary layer between the interface and bulk water.

## II. EXPERIMENTAL PROCEDURES

**II.A. Sample Preparation and Characterization.** AOT [sodium bis(2-ethylhexyl) sulfosuccinate], isooctane, $D_2O$, and potassium selenocyanate (KSeCN) were purchased from Sigma Aldrich and were used as received. A 0.15 M stock solution of AOT in isooctane was prepared and the residual water content in the stock solution was determined using Karl Fischer titration to be ∼0.3 water molecules per AOT ($w_0$ = 0.3). A specific amount of KSeCN in $D_2O$ solution was added to the AOT/isooctane stock solution to achieve the desired $w_0$. The concentration of KSeCN was determined such that the average number of KSeCN anions in one RM is small enough to avoid vibrational excitation transfer. On average, there are four to six KSeCN anions in an individual large RM, whereas the number of water molecules in the RMs ranges from ∼3000 for $w_0$ = 16 to ∼8000 for $w_0$ = 25. In the RMs with $w_0$ = 5, 2, and 1, there are approximately 1, 0.3, and 0.03 KSeCN anions, respectively. For RMs ranging from $w_0$ = 2−20, the water pool diameter is characterized by the formula $d$ (nm) = 0.29$w_0$ + 1.1, which has been determined by a large number of viscosity measurements.[8] For the largest RM, $w_0$ = 25, the diameter was determined by photon correlation spectroscopy (PCS)[34] to be 9 nm, which is within error of the formula. In the experiments, we studied RMs with $w_0$ = 1, 2, 5, 16, 20, and 25, which have diameters of 1.4, 1.7, 2.65, 5.7, 6.9, and 9 nm (PCS or 8.4 nm from the formula), respectively. Viscosity measurements and dynamic light scattering were performed on RM solutions with and without KSeCN. The results showed that the solution viscosities were unchanged and there was no aggregation after the addition of the salt. Therefore, adding the KSeCN probe did not change the properties of the AOT micelle systems.



DOI: 10.1021/acs.jpcb.7b01028
J. Phys. Chem. B 2017, 121, 4530−4537

Samples for IR absorption and ultrafast IR experiments were contained in sample cells composed of two $CaF_2$ windows separated by a Teflon spacer. The thickness of the spacer was selected to have an optical density in the range of 20−200 mOD in the CN stretch region for all samples. $D_2O$ was used instead of $H_2O$ because $H_2O$ has large background absorption in the CN stretch region of $SeCN^-$.

**II.B. PSPP Experiment.** The PSPP experiments were performed using a pulse-shaping IR optical setup.[35] A mid-IR optical parametric amplifier pumped by a Ti:Sapphire regenerative amplifier produced ~170 fs pulses centered at 2075 $cm^{-1}$, with ~30 $\mu$J pulse energy. The mid-IR pulse was then split into a weak probe pulse and a strong pump pulse. The pump pulse passed through an acousto-optic mid-IR Fourier-domain pulse shaper, which was used to phase-cycle and chop the pump beam. The phase cycling reduces the deleterious effects of scattered light. Because of the large transition dipole of the $SeCN^-$ anion, the pump pulse was attenuated to avoid saturation, which distorted the anisotropy data. The probe pulse arrived after a delay time, $t$, which was controlled by a mechanical delay line.

The PSPP experiments track the decay of the probe transmission, with polarizations parallel and perpendicular to the pump-pulse polarization. The parallel and perpendicular components of the probe signal, $S_{\parallel}(t)$ and $S_{\perp}(t)$, respectively, can be expressed in terms of population relaxation, $P(t)$, and the second Legendre polynomial orientational correlation function, $C_2(t)$

$$S_{\parallel}(t) = P(t)[1 + 0.8C_2(t)] \quad (1)$$

$$S_{\perp}(t) = P(t)[1 - 0.4C_2(t)] \quad (2)$$

In terms of these, the population relaxation and reorientational relaxation are

$$P(t) = S_{\parallel}(t) + 2S_{\perp}(t) \quad (3)$$

$$r(t) = \frac{S_{\parallel}(t) - S_{\perp}(t)}{S_{\parallel}(t) + 2S_{\perp}(t)} \quad (4)$$

where $r(t)$ is the anisotropy, with $r(t) = 0.4C_2(t)$.

In the PSPP experiments, the input polarization of the probe was horizontal. A half-wave plate and a polarizer set the polarization of the pump at 45° relative to the horizontal. Following the sample, the probe pulse was resolved either parallel or perpendicular to the polarization of the pump using a polarizer in a computer-controlled rotation mount. Care was taken to make sure that the probe spectra in the parallel and perpendicular polarizations were identical in amplitude in the absence of the pump pulse.

## III. RESULTS AND DISCUSSION

**III.A. Absorption Spectra.** In Figure 1A, FT-IR spectra of the CN stretch of $SeCN^-$ anions in RMs and bulk water are shown. The spectrum in bulk water is centered at 2075 $cm^{-1}$. As the size of the RM decreases, the spectra shift to red. The spectrum for $w_0 = 1$ is centered at 2065 $cm^{-1}$. The spectral shifts are small until $w_0 = 5$ and become pronounced for $w_0 = 2$. In the bulk water solution, the $SeCN^-$ anions are fully solvated by water. In contrast, in the $w_0 = 1$ RMs, the $SeCN^-$ anions mainly interact with the AOT interface. AOT head groups require four to six water molecules for complete hydration.[36]

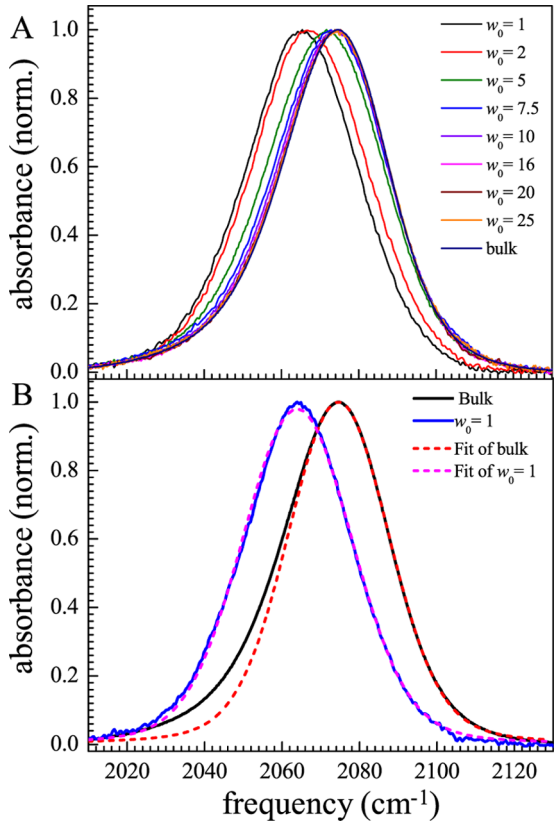


**Figure 1.** (A) IR absorption spectra of the $SeCN^-$ anion in various sizes of RMs (labeled by the $w_0$ parameter) and in bulk water. (B) IR absorption spectra of $SeCN^-$ in bulk water and in the $w_0 = 1$ RM (solid curves) and their fits (dashed curves). The spectrum in $w_0 = 1$ RMs is symmetric, as shown by the excellent fit to a Voigt function. The spectrum in bulk water was fit on the high-frequency side of the line just past the peak and the fit was extended to the red side of the line, showing that the spectrum is not symmetric.

There is so little water that $SeCN^-$ is not solvated and most of these anions do not interact with water.

Figure 1B shows the $SeCN^-$ spectrum in the $w_0 = 1$ RMs and in bulk water along with fits to Voigt functions. The $w_0 = 1$ RM spectrum is perfectly symmetrical. The bulk water spectrum was fit on the blue side of the line and the fit was extended to the red side. The fit curve shows that the bulk water spectrum is not symmetrical. The wing on the red side of the line is likely caused by the non-Condon effect.[37,38] The strength of hydrogen bonding varies across the line. Anions on the red side of the line have increased transition dipoles, which result in the red wing.[27] The non-Condon effect demonstrates the role of hydrogen bonding to $SeCN^-$ in bulk water that is absent in the $w_0 = 1$ RM spectrum. The symmetrical shape of the $w_0 = 1$ RM spectrum supports that the spectrum does not involve significant interactions of the anion with water. Therefore, we take the $w_0 = 1$ RM spectrum to represent that of $SeCN^-$ interacting solely with the interface.

All of the spectra between $w_0 = 1$ RMs and bulk water can be fit by a weighted summation of the $w_0 = 1$ spectrum and the bulk water spectrum. Figure 2A shows the $w_0 = 2$ RM spectrum (black curve) and the fit to the spectrum (dashed magenta curve). The only adjustable parameter is the relative amplitude of the $w_0 = 1$ RM and bulk water spectra. The components of the fit, the $w_0 = 1$ RM spectrum (blue curve) and bulk spectrum (red curve), are also shown. The $w_0 = 1$ RM spectrum is the


DOI: 10.1021/acs.jpcb.7b01028
J. Phys. Chem. B 2017, 121, 4530−4537

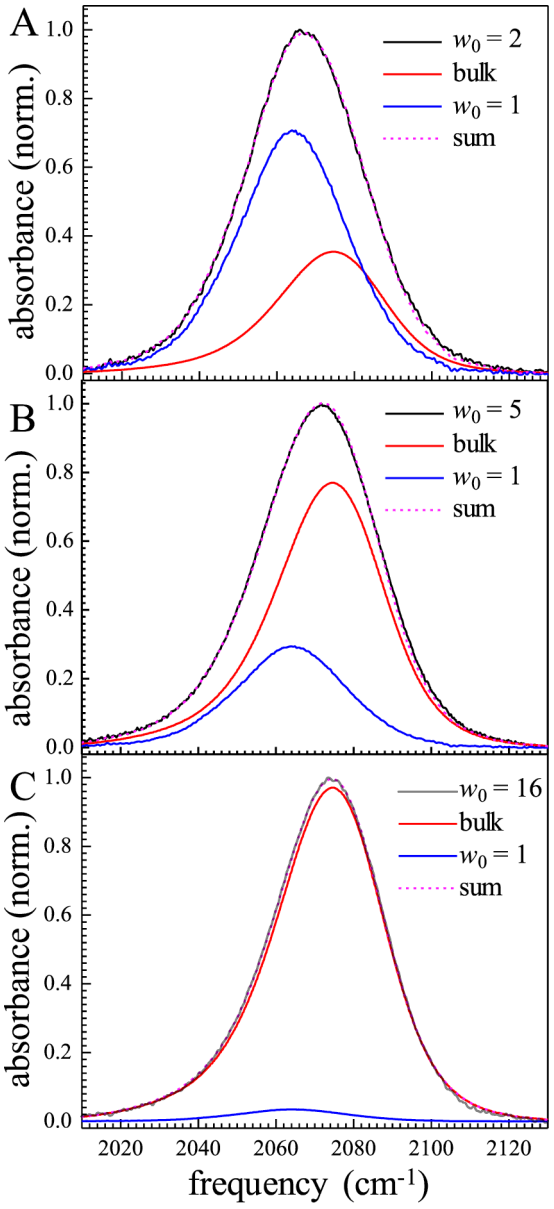


**Figure 2.** IR absorption spectra of $SeCN^-$ in $w_0$ = 2 (A), 5 (B), and 16 (C) RMs (black curves) and their fits (dashed curves) to the sum of the spectra in $w_0$ = 1 RMs and bulk water. Only the amplitudes of these two spectra were varied to fit the spectra. The spectra in $w_0$ = 1 RMs (blue curve) and bulk water (red curve), with the amplitudes obtained from the fits, are shown. All of the spectra in the RMs with $w_0$ = 2–25 can be accurately fit in the manner shown in (A)–(C).

dominant component, but the bulk spectrum is not negligible. It is well established that the $w_0$ = 2 RM does not have a bulk water core[1,2] or enough water to fully hydrate the AOT sulfonate head groups[36] or the $SeCN^-$ anions. The fact that the $SeCN^-$ spectrum of the $w_0$ = 2 RMs can be fit to the sum of the spectra of $w_0$ = 1 RM and bulk water within experimental error suggests that the bulk water spectrum is obtained when a single hydrogen bond is formed between the CN moiety and a water molecule. It is not necessary to fully hydrate the $SeCN^-$ anions to obtain the same spectrum that occurs in bulk water within experimental error. The AOT RMs do not have a bulk water core until they are large, that is, ~$w_0$ = 16 or larger.

Figure 2B presents the $w_0$ = 5 RM spectrum, and it is fit very well using the same method. Again, there is no bulk water in the $w_0$ = 5 RMs[1,2] to fully solvate $SeCN^-$ anions. Therefore, "the bulk" component of the CN stretch spectra for $w_0$ = 2 and 5 RMs is actually the spectrum that arises from formation of a single hydrogen bond with nitrogen. Figure 2C shows the fit to the $SeCN^-$ spectrum in $w_0$ = 16, which contains a bulk water core.[1] For $w_0$ = 16, the spectrum is dominated by the bulk water spectrum, with a very small but necessary contribution from the $w_0$ = 1 RM spectrum. The $w_0$ = 1 component becomes increasingly small as the RMs become larger, and for $w_0$ = 20 and 25, the $w_0$ = 1 component is almost negligible.

**III.B. Polarization-Selective Pump–Probe Experiments.** Figure 3A shows the $SeCN^-$ anisotropy decays extracted from PSPP experiments for the bulk water solution (black points) and $w_0$ = 16 RMs (red points). The anisotropy decay of the $SeCN^-$ anion in bulk water was fit very well with a

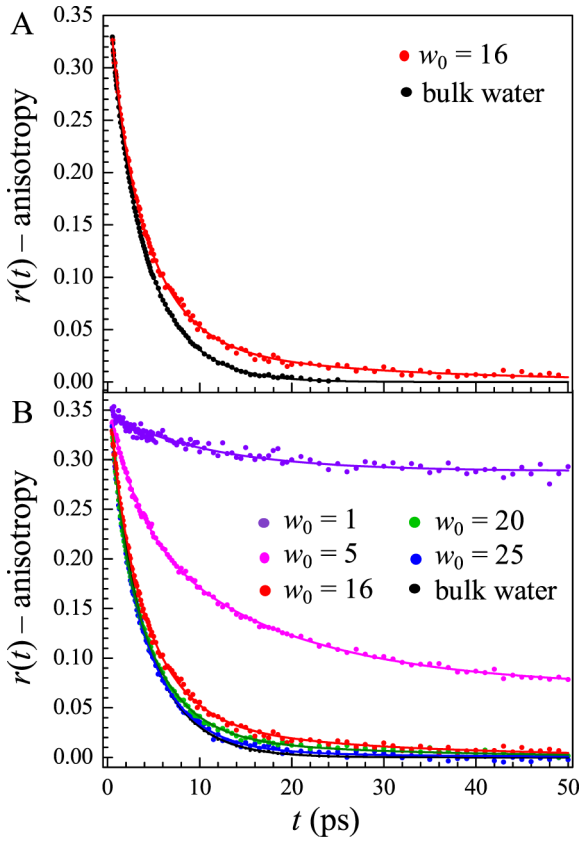


**Figure 3.** (A) Anisotropy decays of $SeCN^-$ in $w_0$ = 16 RMs (red points) and in bulk water (black points) and multiexponential fits. The data for $SeCN^-$ in bulk water fits to a biexponential function with two relatively fast time constants. The data in the $w_0$ = 16 RMs is fit with a triexponential function. The two fast components are the same as those found for bulk water. In addition, there is a relatively small amplitude, a much slower component. (B) Anisotropy decays of $SeCN^-$ in $w_0$ = 1, 5, 16, 20, and 25 RMs and in bulk water (points) and multiexponential fits. For the RMs with $w_0$ = 16, 20, and 25, the two fast components are the same as those found in bulk water. The slow components have the same decay constant within experimental error but have decreasing amplitudes as the RMs become larger. The anisotropy decay for the $w_0$ = 1 RMs is much slower. The decay goes to a large offset, showing that the final orientation relaxation is too slow to measure within the experimental time window set by the vibrational lifetime. The fit to the data in $w_0$ = 5 is a combination of the $w_0$ = 1 decay and biexponential, with the slowest component being much slower than that for the large RMs (see the text for procedure).



DOI: 10.1021/acs.jpcb.7b01028
J. Phys. Chem. B 2017, 121, 4530–4537

biexponential decay. The fit yields two time constants, 1.4 and 4.5 ps (black solid curve). This biexponential anisotropy decay can be analyzed with the wobbling-in-a-cone model.[21,39] The 4.5 ps component is the complete orientational randomization of the $SeCN^-$ anion. The faster time constant reflects orientational sampling in a restricted cone of angles. On the longer time scale, the restrictions that prevent complete sampling are relaxed and the orientation randomizes. Using the wobbling-in-a-cone formalism[21] gives wobbling motion time constant of 2.0 ps and a cone half angle of 21.5°. The data curve extrapolated from back to 0 from the exponential fit is not 0.4, the maximum possible value of anisotropy. The difference is caused by ultrafast inertial motions that are too fast to measure with the pulse durations used in these experiments. The inertial cone half angle is 11.3°.

The decay of the anisotropy data for $w_0$ = 16 RMs is clearly slower than that for bulk water (see Figure 3A). The data for $w_0$ = 16 RMs cannot be fit with a biexponential function, but it fits very well to a triexponential function (red curve). Of particular importance is that the faster two components of the triexponential are identical to those of the bulk water numbers. The difference between the two data sets in Figure 3A is an additional slow component in the data of $w_0$ = 16 RMs. The slow decay time constant is 25 ± 2 ps. These data indicate that there are two ensembles of $SeCN^-$. One of them is the $SeCN^-$ in the bulk water core of the RMs. The other ensemble gives rise to a much slower orientational relaxation time that is clearly not present in bulk water.

The slow component of the anisotropy decay is 9.4% of that of the total. The bulk water anisotropy decay has two components. The fast wobbling component is ~20% of the total of the bulk decay. It is possible that the nonbulk component in the RM has an additional faster wobbling component that is buried under the large amplitude bulk decays. Such an additional component can only increase the fraction of decay that arises from the nonbulk ensemble of $SeCN^-$ in the micelle. However, such a component is unlikely to exist or at most is very small, as the two fast components agree well with the bulk water results within experimental error.

The additional 25 ps slow component of the anisotropy decay observed in the data for the $w_0$ = 16 RMs cannot arise from $SeCN^-$ adsorbed on the wall of the RMs. Inspection of the linear absorption spectrum in Figure 2C shows that the spectral component that arises from the wall of $SeCN^-$ is very small. In addition, careful quantitative absorption measurements show that the $SeCN^-$ wall component has a smaller transition dipole than that of the absorption of $SeCN^-$ in bulk water. The transition dipole of the wall component is 0.86 times that of bulk water component. The absorption (extinction coefficient) depends on the square of the transition dipole, whereas the pump−probe experiment depends on the fourth power of the transition dipole or the square of the extinction coefficient. Therefore, the contribution of the wall component to the pump−probe signal is even smaller than that indicated by the relative amplitudes of the wall and bulk components shown in Figure 2C spectra. Using the amplitude of the wall spectrum at the experimental wavelength, 2075 $cm^{-1}$, and the ratio of the transition dipoles, the 9.4% nonbulk component of the anisotropy decay is too large by a factor of approximately 5 to arise from $SeCN^-$ bound to the wall.

Figure 3B shows the anisotropy data for five RMs, $w_0$ = 1, 5, 16, 20, 25, and bulk water. The decays of the $w_0$ = 1 and 5 RMs are fundamentally different from that of the large RMs and bulk water. In the decays of the $w_0$ = 5, 16, 20, and 25 RMs, the decay component of the $w_0$ = 1 RM contributes to different extents. For the $w_0$ = 5 RM, the contribution is relatively large (see Figure 2B). For the $w_0$ = 16, 20, and 25 RMs, it is minor but makes a difference in analyzing the data.

To rigorously analyze the slow component of the large RMs, the $w_0$ = 1 RM needs to be accounted for. To do this, the two-component version of the anisotropy decay given in eq 4 is employed.[40] The first component (1) is from the $w_0$ = 1 RM contribution, whereas the second component (2) is from the rest of $SeCN^-$ anions in the RMs. The linear absorption spectrum, with differences in the transition dipoles, is used to determine the initial fraction of each component. The expression for total anisotropy, $R(t)$, is

$$R(t) = \frac{f_1 P_1(t) r_1(t) + f_2 P_2(t) r_2(t)}{f_1 P_1(t) + f_2 P_2(t)} \tag{5}$$

$f_1$ and $f_2$ are the fractions of the signals coming from the two components at $t$ = 0. $P_1$ and $P_2$ are the population decays (eq 3), $r_1(t)$ is the anisotropy decay of $SeCN^-$ in the $w_0$ = 1 RMs (purple curve in Figure 3B). The only unknown is the desired $r_2(t)$. For the purposes of fitting, eq 5 was rearranged as follows: $f_1(t)$ and $f_2(t)$ are defined as

$$f_1(t) = \frac{f_1 P_1(t)}{f_1 P_1(t) + f_2 P_2(t)} \quad f_2(t) = \frac{f_2 P_2(t)}{f_1 P_1(t) + f_2 P_2(t)} \tag{6}$$

The eq 5 becomes

$$R(t) = f_1(t) r_1(t) + f_2(t) r_2(t) \tag{7}$$

All of the inputs for the first term on the right-hand side (rhs) of eq 7 are known. It is subtracted from the data, and the remaining data are fit to the second term on the rhs of eq 7. Again, the only unknown is $r_2(t)$. Therefore, the large RM data were fit with $r_2(t)$ as a triexponential, with the two fast components fixed at the bulk water values. Then, the adjustable parameters are the long-component time constant and amplitude.

For $w_0$ = 16, 20, and 25 RMs, the slow components of the anisotropy decay time constants were determined to be 13 ± 1, 13 ± 2, and 13 ± 5 ps, respectively. The error bars on the slow components of the anisotropy decay are larger as the size of the RMs increase because the percentages of decay that arise from the slow components decrease. The percentages are 13.4% for $w_0$ = 16 RMs, 6.2% for $w_0$ = 20 RMs, and 1.2% for $w_0$ = 25 RMs. The very small amplitude of the $w_0$ = 25 component is responsible for the large error bars.

The decrease in the amplitude of the slow component is consistent with the slow component being associated with $SeCN^-$ in a boundary layer that lies between the RM surfactant wall and the bulk water core. As the RMs become larger, the size of the bulk water core increases and the fraction of $SeCN^-$ in the boundary layer decreases.

The $SeCN^-$ anions in the water boundary layer are distinct from the $SeCN^-$ bound to and possibly embedded in the wall. The wall component gives rise to the $w_0$ = 1 RM spectrum, shown in Figure 1B, and is associated with $SeCN^-$ anions that do not have a hydrogen bond to nitrogen. Within experimental error, we cannot distinguish the spectrum of $SeCN^-$ in the boundary layer and in bulk water. All of the spectra from the different-sized RMs are fit exceedingly well by the sum of the $SeCN^-$ spectra in bulk water and $w_0$ = 1 RMs. In addition, the


DOI: 10.1021/acs.jpcb.7b01028
J. Phys. Chem. B 2017, 121, 4530−4537

vibrational lifetime is a single-exponential decay in all of the large RMs and, within experimental error, is the same as that in bulk water. The orientational relaxation of $SeCN^-$ requires water to undergo hydrogen bond rearrangements. The results suggest that the structure of water in the boundary layer is very similar to that of bulk water, that is, essentially a tetrahedral hydrogen bond network, but the hydrogen bond rearrangement is much slower than that in bulk water. The 13 ps orientational relaxation time for $SeCN^-$ in the boundary layer is an average value over the boundary layer. It is reasonable to envision that the water molecules in the boundary layer will be more influenced near the wall, and the effect of the interface will decrease when moving away from the wall. At a large enough distance from the interface, the water has the properties of bulk water.

In small RMs, such as $w_0$ = 5 RMs, a boundary layer will not exist as RMs of this size do not have bulk water cores. The small diameter, 2.6 nm, results in all of the water molecules basically forming a single nonbulk ensemble.[1] Therefore, it would be expected that the nonwall component of the $SeCN^-$ orientational relaxation would be very different from that in the large RMs that have a bulk water core. To test this idea, we determined the anisotropy decay of the nonwall component of the $w_0$ = 5 RM data. A two-component anisotropy model (eq 7) was applied using the $w_0$ = 1 population decay, $P_1(t)$, and its anisotropy decay, $r_1(t)$. Fractions $f_1$ and $f_2$ were obtained from the absorption spectrum (Figure 2B) at the frequency of 2075 $cm^{-1}$ and corrected for the difference in transition dipoles. It is necessary to know $P_2(t)$. To obtain $P_2(t)$, we fit the $w_0$ = 5 population decay data at 2075 $cm^{-1}$ using the known $P_1(t)$ and an additional exponential representing $P_2(t)$. The result is that $P_2(t)$ gives the same single-exponential decay found for bulk water and the large RMs with an experimental error. This is an interesting result. As discussed immediately below, $r_2(t)$ is much slower than that found for the boundary layers in the large RMs, but the population decay is the same. The population decay depends on the local solvation structure of the water molecules surrounding the vibrationally excited $SeCN^-$. Thus, for vibrational relaxation, the coupling of the CN stretch in the nonwall component of $w_0$ = 5 RMs is slightly different from its coupling in bulk water.

The anisotropy decay $w_0$ = 5 RMs was fit as discussed above. The nonwall component required a biexponential function to fit the data. The two components had decay constants of 4.7 and 35 ps when the data were fit with no offset. However, the data could also be fit with an offset. An offset indicates that there is a component that is so slow that it is outside of the experimental time window determined by the vibrational lifetime. Therefore, the fastest that the complete orientational relaxation can be is 35 ps, and it is possible that it is much slower. The 35 ps or a slower decay should be compared with the boundary layer anisotropy decay of 13 ps. As anticipated, for the small RMs that do not have a bulk water core and therefore, no boundary layer, the orientational relaxation is much slower.

If it is assumed that $SeCN^-$ are randomly distributed in the water nanopool, the width of the boundary layer is obtained by finding the volume of a thin spherical shell that contains the correct fraction of $SeCN^-$ anions, as determined by the amplitude of the slow component of the anisotropy. When this is done for $w_0$ = 16 RMs, the width of the shell becomes 1.3 Å. This width is physically impossible as it is ~46% of the diameter of one water molecule (~2.8 Å). $SeCN^-$, which is much larger than a water molecule, cannot be in a layer with a width much less than the size of a water molecule. The same geometrical calculations show that the shell width would have to be even smaller to account for the slow anisotropy component of the larger RMs.

The simple geometrical calculations indicate that $SeCN^-$ is repelled by the interface, which is lined with negatively charged sulfonate head groups. Simulations have shown that for small AOT RMs ions added to the water pool are repelled by the sulfonate-lined interface.[41] Although the sulfonates are on the surface of the interface, at least some of the $Na^+$ counterions tend to be away from the interface and solvated by water. The repulsion of $SeCN^-$ by the interface can be understood in terms of the Gouy−Chapman model.[42−44] In an ideal Gouy−Chapman model, the sulfonate head groups with a negative charge are arrayed on the interface and the counterions, $Na^+$ cations, have a gradient of decreasing concentration as the distance from the interface increases. This model will generate an electrostatic field that repels the $SeCN^-$ anions from the interface. Anions were also found to be repelled from the interface in other studies.[45,46] Note that even at very high concentrations of salts such as NaCl in water, a singly charged cation like $Na^+$ does not have a significant effect on water dynamics.[47] Therefore, $Na^+$ or other singly charged cations are unlikely to be the source of the boundary layer and the slower dynamics within it.

Because $SeCN^-$ are not randomly distributed, a simple geometric calculation based on the ratio of the amplitude of the slow component of the anisotropy to the amplitude of the combined fast components is not sufficient to determine the width of the boundary layer. For AOT RMs with $w_0$ = 16 and larger, it has been determined that there was a core of water with bulk water properties.[1] The experiments were conducted on the OD stretch of the low concentration of HOD in $H_2O$. Both the orientational relaxation time and the OD stretch lifetime were found to be the same as bulk water for water molecules not associated with the wall. RMs with $w_0$ = 16 have water-pool diameters of 5.7 nm. For $w_0$ = 10 RMs, with a diameter of 4 nm, it was determined that there was still a core with distinct dynamics from water directly interacting with the interface. However, the core no longer was strictly bulklike. Both the HOD orientational relation time and the OD stretch lifetime in the core were close to but somewhat longer than the bulk water values.[1] These results were interpreted as indicating that the influence of the interface extended to ~2 nm. Simulations and measurements on various systems discussed in the Introduction indicate boundary layer widths of ~1 nm. Therefore, the width of the boundary layer is likely between 1 and 2 nm, with $SeCN^-$ repelled from the immediate vicinity of the interface.

## IV. CONCLUDING REMARKS

We have experimentally observed a water boundary layer that lies between the surfactant/water interface and bulk water core in large AOT RMs. A small anion, $SeCN^-$, was used as a vibrational probe. Polarization-selective pump−probe experiments were used to measure the orientation relaxation (anisotropy decay) of the anion. In bulk water, $SeCN^-$ displays two anisotropy decay components, a 1.4 ps wobbling motion and a 4.5 ps complete orientational randomization time constant. In large RMs, which have a bulk water core, the two bulk water time constants, and additional ~13 ps anisotropy decay were observed. This additional slow relaxation



DOI: 10.1021/acs.jpcb.7b01028
J. Phys. Chem. B 2017, 121, 4530−4537

component was assigned to $SeCN^-$ in the boundary layer between the interface and bulk water core.

The additional slow component of the anisotropy decay has a time constant that is similar for the three different-sized RMs, $w_0$ = 16, 20, and 25, that were studied. As the RM size is increased, the amplitude of the slow component relative to that of the bulk water components decreases. The decrease in amplitude with increasing size is consistent with a boundary layer that becomes a smaller fraction of the total RM water pool as the size increases. The results also suggest that $SeCN^-$ is not randomly distributed in the water nanopool, but rather is repelled from the interface that is lined with sulfonate anionic head groups. The repulsion of the $SeCN^-$ anions from the interface can be understood in terms of the Gouy−Chapman model.[42−44]

For orientational relaxation to occur, the solvating water hydrogen bond network must rearrange. The results show that in the boundary layer the water hydrogen bond network dynamics are slower than in bulk water. Although the orientational relaxation in the boundary layer is substantially slower, within experimental error, the absorption spectrum and the vibrational lifetime of the CN stretch of $SeCN^-$ are the same in bulk water and in the boundary layer. The lack of a change in the spectrum and lifetime indicates that the interactions between $SeCN^-$ and the surrounding water in the boundary layer are essentially the same as they are in bulk water. Therefore, the structure of the water hydrogen bond network in the boundary layer is not significantly different from that of bulk water, although the time scale for hydrogen bond rearrangement is slower. We also performed 2D IR vibrational echo experiments on $SeCN^-$ in bulk water[27] and in the large RMs. The 2D IR experiments measure spectral diffusion, which is caused by the water hydrogen bond dynamics. In bulk water, the slowest component of the spectral diffusion is ∼1.5 ps. In the RMs, an additional slow component of ∼12 ps was observed. This observation is consistent with the interpretation of the 13 ps anisotropy component as arising from slower water dynamics in the boundary layer.

## AUTHOR INFORMATION


### Corresponding Author

*Email: fayer@stanford.edu. Phone: 650 723-4446.

### ORCID

Michael D. Fayer: 0000-0002-0021-1815


### Notes

The authors declare no competing financial interest.

## ACKNOWLEDGMENTS

We thank Professor Nancy Levinger and her co-workers at Colorado State University for performing Dynamic Light Scattering experiments that confirmed that the RMs were not aggregating. This work was supported by the Air Force Office of Scientific Research grant number FA9550-16-1-0104 (C.Y., J.N., and M.D.F.) and by the Division of Chemical Sciences, Geosciences, and Biosciences, Office of Basic Energy Sciences of the U.S. Department of Energy (DOE) grant number DE-FG03-84ER13251 (R.Y. and M.D.F.).

## REFERENCES


(1) Moilanen, D. E.; Fenn, E. E.; Wong, D.; Fayer, M. D. Water Dynamics in Large and Small Reverse Micelles: From Two Ensembles to Collective Behavior. *J. Chem. Phys.* **2009**, *131*, No. 014704.

(2) Pieniazek, P. A.; Lin, Y.-S.; Chowdhary, J.; Ladanyi, B. M.; Skinner, J. L. Vibrational Spectroscopy and Dynamics of Water Confined inside Reverse Micelles. *J. Phys. Chem. B* **2009**, *113*, 15017−15028.

(3) Pileni, M. P. Reverse Micelles as Microreactors. *J. Phys. Chem.* **1993**, *97*, 6961−6973.

(4) Qian, Y. D.; Wen, W.; Adcock, P. A.; Jiang, Z.; Hakim, N.; Saha, M. S.; Mukerjee, S. Ptm/C Catalyst Prepared Using Reverse Micelle Method for Oxygen Reduction Reaction in Pem Fuel Cells. *J. Phys. Chem. C* **2008**, *112*, 1146−1157.

(5) Zarur, A. J.; Ying, J. Y. Reverse Microemulsion Synthesis of Nanostructured Complex Oxides for Catalytic Combustion. *Nature* **2000**, *403*, 65−67.

(6) Luisi, P. L.; Giomini, M.; Pileni, M. P.; Robinson, B. H. Reverse Micelles as Hosts for Proteins and Small Molecules. *Biochim. Biophys. Acta* **1988**, *947*, 209−246.

(7) Luisi, P. L. Enzymes Hosted in Reverse Micelles in Hydrocarbon Solution. *Angew. Chem., Int. Ed. Engl.* **1985**, *24*, 439−528.

(8) Kinugasa, T.; Kondo, A.; Nishimura, S.; Miyauchi, Y.; Nishii, Y.; Watanabe, K.; Takeuchi, H. Estimation for Size of Reverse Micelles Formed by AOT and Sdehp Based on Viscosity Measurement. *Colloids Surf., A* **2002**, *204*, 193−199.

(9) Vasquez, V. R.; Williams, B. C.; Graeve, O. A. Stability and Comparative Analysis of AOT/Water/Isooctane Reverse Micelle System Using Dynamic Light Scattering and Molecular Dynamics. *J. Phys. Chem. B* **2011**, *115*, 2979−2987.

(10) Eskici, G.; Axelsen, P. H. The Size of AOT Reverse Micelles. *J. Phys. Chem. B* **2016**, *120*, 11337−11347.

(11) Grigolini, P.; Maestro, M. A Two-State Stochastic Model for the Dynamics of Constrained Water in Reversed Micelles. *Chem. Phys. Lett.* **1986**, *127*, 248−252.

(12) Quist, P.-O.; Halle, B. Water Dynamics and Aggregate Structure in Reversed Micelles at Sub-Zero Temperatures. *J. Chem. Soc., Faraday Trans. 1* **1988**, *84*, 1033−1046.

(13) Pant, D.; Riter, R. E.; Levinger, N. E. Influence of Restricted Environment and Ionic Interactions on Water Solvation Dynamics. *J. Chem. Phys.* **1998**, *109*, 9995−10003.

(14) Douhal, A.; Angulo, G.; Gil, M.; Organero, J. A.; Sanz, M.; Tormo, L. Observation of Three Behaviors in Confined Liquid Water within a Nanopool Hosting Proton-Transfer Reactions. *J. Phys. Chem. B* **2007**, *111*, 5487−5493.

(15) Riter, R. E.; Willard, D. M.; Levinger, N. E. Water Immobilization at Surfactant Interfaces in Reverse Micelles. *J. Phys. Chem. B* **1998**, *102*, 2705−2714.

(16) Harpham, M. R.; Ladanyi, B. M.; Levinger, N. E.; Herwig, K. W. Water Motion in Reverse Micelles Studied by Quasielastic Neutron Scattering and Molecular Dynamics Simulations. *J. Chem. Phys.* **2004**, *121*, 7855.

(17) Bradley-Shaw, J. L.; Camp, P. J.; Dowding, P. J.; Lewtas, K. Glycerol Monooleate Reverse Micelles in Nonpolar Solvents: Computer Simulations and Small-Angle Neutron Scattering. *J. Phys. Chem. B* **2015**, *119*, 4321−4331.

(18) D'Angelo, M.; Fioretto, D.; Onori, G.; Palmieri, L.; Santucci, A. Dynamics of Water-Containing Sodium Bis(2-Ethylhexyl)-Sulfosuccinate (AOT) Reverse Micelles: A High-Frequency Dielectric Study. *Phys. Rev. E* **1996**, *54*, 993−996.

(19) Faeder, J.; Ladanyi, B. M. Molecular Dynamics Simulations of the Interior of Aqueous Reverse Micelles. *J. Phys. Chem. B* **2000**, *104*, 1033−1046.

(20) Abel, S.; Sterpone, F.; Bandyopadhyay, S.; Marchi, M. Molecular Modeling and Simulations of AOT-Water Reverse Micelles in Isooctane: Structural and Dynamic Properties. *J. Phys. Chem. B* **2004**, *108*, 19458−19466.

(21) Tan, H.-S.; Piletic, I. R.; Fayer, M. D. Orientational Dynamics of Water Confined on a Nanometer Length Scale in Reverse Micelles. *J. Chem. Phys.* **2005**, *122*, No. 174501.

(22) Dokter, A. M.; Woutersen, S.; Bakker, H. J. Anomalous Slowing Down of the Vibrational Relaxation of Liquid Water Upon Nanoscale Confinement. *Phys. Rev. Lett.* **2005**, *94*, No. 178301.




DOI: 10.1021/acs.jpcb.7b01028
J. Phys. Chem. B 2017, 121, 4530−4537

(23) Moilanen, D. E.; Fenn, E. E.; Wong, D.; Fayer, M. D. Water Dynamics in AOT Lamellar Structures and Reverse Micelles: Geometry and Length Scales Vs. Surface Interactions. *J. Am. Chem. Soc.* **2009**, *131*, 8318−8328.
(24) Fenn, E. E.; Wong, D. B.; Giammanco, C. H.; Fayer, M. D. Dynamics of Water at the Interface in Reverse Micelles: Measurements of Spectral Diffusion with Two-Dimensional Infrared Vibrational Echoes. *J. Phys. Chem. B* **2011**, *115*, 11658−11670.
(25) Moilanen, D. E.; Fenn, E. E.; Wong, D.; Fayer, M. D. Water Dynamics at the Interface in AOT Reverse Micelles. *J. Phys. Chem. B* **2009**, *113*, 8560−8568.
(26) Moilanen, D. E.; Levinger, N.; Spry, D. B.; Fayer, M. D. Confinement or the Nature of the Interface? Dynamics of Nanoscopic Water in Reverse Micelles. *J. Am. Chem. Soc.* **2007**, *129*, 14311−14318.
(27) Yuan, R.; Yan, C.; Tamimi, A.; Fayer, M. D. Molecular Anion Hydrogen Bonding Dynamics in Aqueous Solution. *J. Phys. Chem. B* **2015**, *119*, 13407−13415.
(28) Loparo, J. J.; Roberts, S. T.; Tokmakoff, A. Multidimensional Infrared Spectroscopy of Water. I. Vibrational Dynamics in Two-Dimensional IR Line Shapes. *J. Chem. Phys.* **2006**, *125*, No. 194521.
(29) Abel, S.; Galamba, N.; Karakas, E.; Marchi, M.; Thompson, W. H.; Laage, D. On the Structural and Dynamical Properties of DOPC Reverse Micelles. *Langmuir* **2016**, *32*, 10610−10620.
(30) Goertz, M. P.; Houston, J. E.; Zhu, X. Y. Hydrophilicity and the Viscosity of Interfacial Water. *Langmuir* **2007**, *23*, 5491−5497.
(31) Asay, D. B.; Kim, S. H. Evolution of the Adsorbed Water Layer Structure on Silicon Oxide at Room Temperature. *J. Phys. Chem. B* **2005**, *109*, 16760−16763.
(32) Cheng, L.; Fenter, P.; Nagy, K. L.; Schlegel, M. L.; Sturchio, N. C. Molecular-Scale Density Oscillations in Water Adjacent to a Mica Surface. *Phys. Rev. Lett.* **2001**, *87*, No. 156103.
(33) Singh, P. K.; Kuroda, D. G.; Hochstrasser, R. M. An Ion's Perspective on the Molecular Motions of Nanoconfined Water: A Two-Dimensional Infrared Spectroscopy Study. *J. Phys. Chem. B* **2013**, *117*, 9775−9784.
(34) Zulauf, M.; Eicke, H. F. Inverted Micelles and Microemulsions in the Ternary-System $H_2O$-Aerosol-OT-Isooctane as Studied by Photon Correlation Spectroscopy. *J. Phys. Chem.* **1979**, *83*, 480−486.
(35) Kumar, S. K. K.; Tamimi, A.; Fayer, M. D. Comparisons of 2D IR Measured Spectral Diffusion in Rotating Frames Using Pulse Shaping and in the Stationary Frame Using the Standard Method. *J. Chem. Phys.* **2012**, *137*, No. 184201.
(36) Hauser, H.; Haering, G.; Pande, A.; Luisi, P. L. Interaction of Water with Sodium Bis(2-Ethyl-1-Hexyl) Sulfosuccinate in Reversed Micelles. *J. Phys. Chem.* **1989**, *93*, 7869−7876.
(37) Schmidt, J. R.; Corcelli, S. A.; Skinner, J. L. Pronounced Non-Condon Effects in the Ultrafast Infrared Spectroscopy of Water. *J. Chem. Phys.* **2005**, *123*, No. 044513.
(38) Lindquist, B. A.; Corcelli, S. A. Nitrile Groups as Vibrational Probes: Calculations of the C≡N Infrared Absorption Line Shape of Acetonitrile in Water and Tetrahydrofuran. *J. Phys. Chem. B* **2008**, *112*, 6301−6303.
(39) Lipari, G.; Szabo, A. Effect of Librational Motion on Fluorescence Depolarization and Nuclear Magnetic-Resonance Relaxation in Macromolecules and Membranes. *Biophys. J.* **1980**, *30*, 489−506.
(40) Piletic, I. R.; Moilanen, D. E.; Spry, D. B.; Levinger, N. E.; Fayer, M. D. Testing the Core/Shell Model of Nanoconfined Water in Reverse Micelles Using Linear and Nonlinear IR Spectroscopy. *J. Phys. Chem. A* **2006**, *110*, 4985−4999.
(41) Faeder, J.; Ladanyi, B. M. Solvation Dynamics in Reverse Micelles: The Role of Headgroup-Solute Interactions. *J. Phys. Chem. B* **2005**, *109*, 6732−6740.
(42) McLaughlin, S. Electrostatic Potentials at Membrane-Solution Interfaces. In *Current Topics in Membranes and Transport*; Felix, B., Arnort, K., Eds.; Academic Press, 1977; Vol. *9*, pp 71−144.
(43) Gawrisch, K.; Ruston, D.; Zimmerberg, J.; Parsegian, V. A.; Rand, R. P.; Fuller, N. Membrane Dipole Potentials, Hydration Forces, and the Ordering of Water at Membrane Surfaces. *Biophys. J.* **1992**, *61*, 1213−1223.
(44) Cafiso, D.; Mclaughlin, A.; Mclaughlin, S.; Winiski, A. Measuring Electrostatic Potentials Adjacent to Membranes. *Methods Enzymol.* **1989**, *171*, 342−364.
(45) Karukstis, K. K.; Frazier, A. A.; Martula, D. S.; Whiles, J. A. Characterization of the Microenvironments in AOT Reverse Micelles Using Multidimensional Spectral Analysis. *J. Phys. Chem.* **1996**, *100*, 11133−11138.
(46) Lawler, C.; Fayer, M. D. Proton Transfer in Ionic and Neutral Reverse Micelles. *J. Phys. Chem. B* **2015**, *119*, 6024−6034.
(47) Giammanco, C. H.; Wong, D. B.; Fayer, M. D. Water Dynamics in Divalent and Monovalent Concentrated Salt Solutions. *J. Phys. Chem. B* **2012**, *116*, 13781−13792.


DOI: 10.1021/acs.jpcb.7b01028
*J. Phys. Chem. B* 2017, 121, 4530−4537